JOURNAL OF PHYSICAL ORGANIC CHEMISTRY
J. Phys. Org. Chem. 2003; **16:** 731–745
Published online in Wiley InterScience (www.interscience.wiley.com). DOI: 10.1002/poc.658

Aromaticity and antiaromaticity: what role do ionic configurations play in delocalization and induction of magnetic properties?

Avital Shurki,[1] Philippe C. Hiberty,[2] Fokke Dijkstra[3] and Sason Shaik[1]*

[1]Department of Organic Chemistry and Lise Meitner-Minerva Center for Computational Quantum Chemistry, The Hebrew University, Jerusalem 91904, Israel
[2]Laboratoire de Chimie Physique, Groupe de Chimie Théorique, Université de Paris-Sud, 91405 Orsay Cédex, France
[3]Theoretical Chemistry Group, Debye Institute, Utrecht University, Padualaan 14, 3584 CH Utrecht, The Netherlands

Received 4 December 2002; revised 28 March 2003; accepted 31 March 2003

epoc ABSTRACT: C_mH_m ($m = 4, 6, 8$) species are analyzed in D_{mh} and $D_{(1/2)mh}$ geometries by means of valence bond (VB) calculations. The fundamental factors that distinguish aromatic and antiaromatic modes of electron delocalization are elucidated by analysis of the mixing between the covalent-state and ionic structures that distribute the electrons in all possible modes available in the cycle. The major difference found is that, by contrast to the aromatic species where all the ionic structures mix into the covalent state, in the antiaromatic species the set of diagonal-ionic structures is excluded from mixing with the covalent-state, owing to its fundamental symmetry features. This exclusion of covalent–ionic mixing is expressed at the most fundamental building blocks of the wavefunction; the spin-alternant state. The spin-alternant state is a resonance hybrid of the two spin-alternant determinants. This resonance hybrid will support a collective motion of the p_π-electrons around the perimeter of the ring only if ionic structures can mix to mediate the electronic flow. It is shown that in aromatic species all the ionic structures mix and sustain a continuous electronic flow around the ring perimeter. By contrast, owing to the exclusion of the diagonal-ionic structures in antiaromatic compounds, the electronic flow in antiaromatic species is interrupted. Symmetry and angular momentum analyses of the ground state in the presence of an external magnetic field show that the properties of the spin-alternant state can qualitatively describe the magnetic properties of the two classes. The continuous flow of π-electrons mediated by the ionic structures of aromatic species is responsible for the enhanced diamagnetism of these species. By contrast, paramagnetic π-ring current in antiaromatic species becomes possible only in the presence of the magnetic field that allows the mixing of the otherwise excluded ionic structures. Copyright © 2003 John Wiley & Sons, Ltd.
Additional material for this paper is available from the epoc website at http://www.wiley.com/epoc

KEYWORDS: aromaticity; antiaromaticity; ionic configurations; delocalization; induction; magnetic properties; valence bond

INTRODUCTION

Despite the extensive research efforts dedicated to the study of aromatic/antiaromatic compounds (for a few summeries of this field, see Ref. 1), the underlying reasons for the different delocalization patterns associated with the $4n + 2/4n$ division and their physical probes[2] continue to engage the interest of chemists.[1e,3] Hückel MO theory[4] shows that species with $4n + 2$ π-electrons, termed aromatic,[1f] are characterized by uniform geometries (equal C—C distances) and are bond delocalized, whereas singlet species with $4n$ π electrons, termed antiaromatic,[1f] are normally characterized by non-uniform geometries and a propensity towards bond localization. Furthermore, aromatic species exhibit enhanced diamagnetic susceptibility relative to a localized reference with the same number of π-electrons, while the antiaromatic species exhibit enhanced paramagnetic susceptibility relative to their localized reference species.[1,5–7] These magnetic properties are typical of the number of π-electrons in the cycle and are expressed even when the two molecular types are considered at their uniform geometries with equal C—C bond lengths, where for all practical purposes the π-electron density is uniformly delocalized over the perimeter of the rings[7,8] (for results on cyclooctatetraene, see Ref. 9; M. Kertesz and K. S. Choi, personal communication regarding unpublished data for *s*-indacene). Clearly, the state of 'bond delocalization' must have different manifestations in aromatic and antiaromatic species, and hence the meaning of 'bond delocalization' for these two classes merits a precise definition.

To appreciate this need further, consider the vertical resonance energies (note that the vertical resonance

**Correspondence to:* S. Shaik, Department of Organic Chemistry and Lise Meitner-Minerva Center for Computational Quantum Chemistry, The Hebrew University, Jerusalem 91904, Israel.
Contract/grant sponsor: Ministry of Science and Culture of the State of Niedersachsen.
Contract/grant sponsor: Robert Szold.

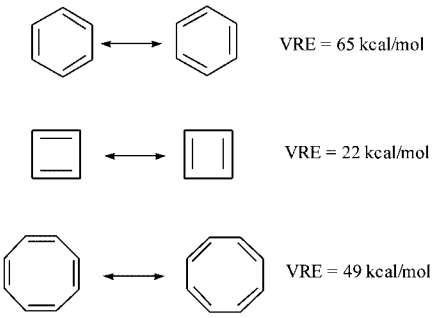

Scheme 1. Vertical resonance energies (VREs) calculated by valence bond (Ref. 10) for benzene, CBD and COT in their uniform D_{mh} geometries (with equal C—C bond lengths)

energies are related to the commonly used Dewar resonance energies, which are positive for aromatic species and negative for antiaromatic ones)[10] due to mixing of the two equivalent Kekulé structures of benzene, cyclobutadiene and cyclooctatetraene at their uniform geometries in Scheme 1. These values, recently computed by us,[10] are in good accord with the experimental estimate of Hornig for the vertical resonance energy of benzene[11] (experimental estimate: VRE = 65 kcal for benzene) and with the RGVB computed datum of Voter and Goddard[12] for cyclobutadiene. It is apparent that the two Kekulé forms mix in all the three species with significant resonance energies, and as such all the species are bond delocalized, having a uniform distribution of the π-electrons around their perimeters. Nevertheless, the aromatic and antiaromatic species exhibit strikingly different magnetic properties. What is the reason for this difference? Does it reflect some intrinsic property of the delocalized π-species that is different for the aromatic and antiaromatic species? It is important to grapple with these questions in order to establish the magnetic property as a probe of the mode of delocalization.[2,3f,6] Molecular orbital (MO) theory ascribes these differences to the closed-shell electronic structure of benzene as opposed to the open-shell structure of singlet cyclobutadiene and cyclooctatetraene, due to orbital degeneracy in the D_{mh} symmetries of the latter two species. While this explanation holds perfectly for the above species, it is less obvious for species such as *s*-indacene, pentalene and others, which have no orbital degeneracy (M. Kertesz and K. S. Choi, personal communication; *s*-indacene) but nevertheless possess magnetic properties typical of antiaromatic species. There must be some more fundamental factor that underlies the different magnetic manifestations of these bond-delocalized species. Such a fundamental factor may be uncovered by the use of valence bond (VB) theory, which often provides complementary insight to MO theory. The present paper tackles these problems from the VB perspective, by going to the fundamental definition of electronic localization, namely delocalization in one bond.

An appreciation of the fundamental meaning of delocalization, viz. localization, can be gained by reviewing the VB description of the simplest of all molecules, H_2, in **1**–**3**. Structure **1** is the covalent structure, made from two spin alternant determinants, which will feature highly later. The electrons in this structure are localized in the sense that they are restricted to occupy one-centered atomic orbitals, even if electron spins switch their location. The other structures **2** and **3** are ionic, and each of them, by itself, describes a localized electron distribution. In the Hartree–Fock (HF) MO wavefunction, the electrons occupy an orbital which is delocalized over the two atomic centers, and in this sense the electrons are delocalized. In VB terms, this delocalization of the HF wavefunction is manifested by the fact that the weights of **1** and those of **2** + **3**, are precisely equal. This means that the electrons in the HF-MO wavefunction have equal probability to be in all the available modes of distribution.

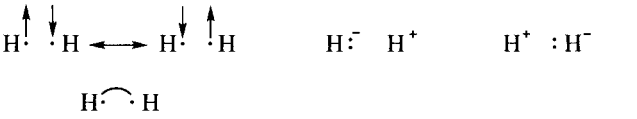

1 **2** **3**

In this sense, the electrons in the HF-MO description of H_2 are completely delocalized. After inclusion of electron correlation by means of configuration interaction (CI), the energy of H_2 decreases, and expansion of the MO-CI wavefunction into VB structures reveals that the weight of the covalent structure **1** grows at the expense of the ionic structures. The electrons are no longer distributed with equal probability in all the modes, but prefer the covalent localized mode. Thus, whereas the covalent–ionic resonance (**1** ↔ **2** + **3**) tends to delocalize the electrons in the bond, the Coulomb repulsion operates in the opposite direction and keeps the electrons apart as in the covalent structure **1**. Consequently, the ionic–covalent mixing and the extent of electronic delocalization both decrease owing to electronic correlation. In this manner, VB theory provides a clear picture of electronic delocalization in a two-center, two-electron bond: electronic delocalization in a single bond is a measure of the extent of mixing of ionic structures into the purely localized covalent structures.

The same trend applies also to the MO and MO-CI wavefunctions of aromatic and antiaromatic species, which can be re-expressed in terms of combinations of covalent and ionic structures. Using the VB perspective, we shall probe the covalent–ionic mixing in a set of aromatic and antiaromatic molecules, C_mH_m ($m = 4, 6, 8$) and try to establish similarities and differences in the modes of delocalization. Subsequently, we shall attempt to link the features of delocalization to the magnetic properties of the two classes. Our treatment has significant affinity with an early treatment of McWeeny,[13] who interpreted the enhanced diamagnetic susceptibility of aromatic compounds by invoking electron hopping due to covalent–ionic mixing. A visual mechanism for diamagnetic ring current[6,14,15] in aromatic molecules will be

suggested, and the origins of the ever-problematic paratropicity in antiaromatics will be derived, based on the covalent–ionic mixing paradigm.

COMPUTATIONAL DETAILS

Programs

The VB calculations were carried out using the Utrecht package TURTLE.[16] This is a general non-orthogonal CI program which performs simultaneously linear variation as well as orbital optimization on a given set of VB configurations. The orbital optimization is based on the super-CI technique[17] related to the generalized Brillouin theorem.[18] The *ab initio* MO and CASSCF calculations were performed with the Gaussian 94[19] and MOLPRO-2000[20,21] packages of programs.

MO and CASSCF studies

The target molecules used in the study were C_4H_4, C_6H_6 and C_8H_8. A partial treatment of $C_{10}H_{10}$ was also carried out. These molecules were constrained to be planar and their geometries were optimized only at the uniform D_{mh} symmetry ($m = 4$, 6, 8, 10, respectively). The aromatic species were optimized at the HF/6–31G level and the antiaromatic species at the CASSCF(n_π/8)/6–31G level (n_π is the number of π-electrons in C_4H_4 and C_8H_8). The following uniform C—C distances where obtained: C_4H_4 1.451, C_6H_6 1.388, C_8H_8 1.402 and $C_{10}H_{10}$ 1.391 Å. The bond alternated geometries at the $D_{(1/2)mh}$ symmetry were obtained by alternately elongating and shortening the C—C bonds of the uniform geometries by a constant increment of 0.05 Å.

VB calculations

Test VB calculations carried out with both the STO-3G and 6–31G basis sets for CBD and benzene showed similar trends. Since our goal is to gain insight, the STO-3G basis was deemed sufficient for the larger systems (C_8H_8 and $C_{10}H_{10}$).

In all VB calculations, the σ-electrons were placed in doubly occupied molecular orbitals. For all systems except for 10-annulene, the σ-orbitals were allowed to optimize and adapt to the π-electrons. The calculation of 10-annulene used frozen doubly occupied MOs as the σ-orbitals. The π-electrons for all systems were placed in singly occupied orbitals and treated at the VB level using atomic orbitals (AOs). Whenever a classical VB structure, e.g. covalent or ionic, was desired the AOs were kept localized on their respective centers. When more compact VB wavefunctions were required, the AOs were allowed to optimize freely, giving rise to p_π-orbitals with small delocalization tails into neighboring fragments. These semi-localized AOs, usually referred to as Coulson Fischer (CF) orbitals,[22] are used in GVB theory and spin coupled (SC) theory, etc.[12,23–26] In the case of the D_{mh} cycles, the delocalization tails are spread in a symmetric fashion on the ring as shown, for example, in **4a** and **4b** for benzene and cyclobutadiene, respectively. The wavefunction of a VB configuration that uses CF orbitals contains contribution from other configurations. In fact, the formally covalent wavefunction with the CF type of orbitals includes a mixture of classical covalent and ionic configurations with localized AOs.[27]

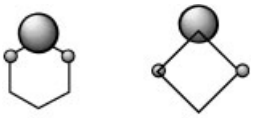

4a **4b**

All the orbitals (σ and π) were optimized self-consistently for the covalent states, spanned by the two principal Kekulé structures of the species (see Scheme 1). These orbitals were then used as a basis for the VB-π-CI calculations that included other structures.

The VB program TURTLE[16] is flexible and it can use either VB structures which are spin eigenfunctions (of $\boldsymbol{S}^2$), or VB determinants which are eigenfunctions only of $\boldsymbol{S}_z$, as the building blocks of the wavefunction. To establish the role of covalent–ionic mixing, we must first construct the covalent state from the covalent structures, and subsequently mix in the complete set of ionic structures. Comparison of the properties of the covalent state and the full state may then reveal the influence of covalent–ionic mixing. Since the number of ionic structures increases very steeply with the number of π-electrons [18 for CBD ($4\pi e^-$), 170 for benzene ($6\pi e^-$), 1750 for COT (8pe−), etc.], a more compact analysis is necessary to reveal trends in a tractable manner. Since the use of CF orbitals in the VB structures is known effectively to involve the ionic structures within the formally covalent wavefunction,[27] separate calculations of covalent-type wavefunctions using localized and then CF orbitals will provide information regarding the ionic mixing into a pure covalent configuration.

RESULTS AND DISCUSSION

Delocalization in aromatic and antiaromatic species

The covalent state. The covalent state for C_mH_m is made up of a linear combination of the covalent Rumer structures, which constitute all the possible ways of pairing the m electrons that occupy the m p_π AOs into $m/2$ pairs.[28] This is exemplified in Scheme 2 for cyclobutadiene and benzene. In cyclobutadiene with four electrons, there are only two modes of pairing, shown

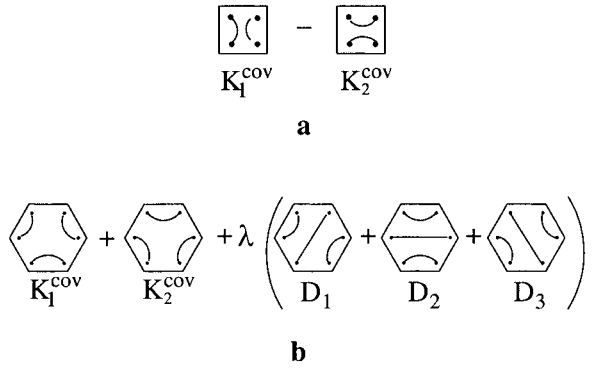

Scheme 2. Pictorial representations of the covalent state of (**a**) CBD and (**b**) benzene

in **a**. In benzene with six electrons, there are five pairing modes, shown in **b**. Two of the forms involve only short bonds and are the familiar covalent Kekulé structures. The other three are the covalent Dewar structures that have one long bond. Detailed VB calculations for benzene show that the Dewar structures, which are of higher energy than the Kekulé structures, make only a small contribution to the stabilization of the ground state. The higher members of the series ($m = 8$, 10) also have two structures with short bonds, and increasing numbers of other Rumer structures[28] with long bonds, which are of higher energy and will not be considered for qualitative purposes. To keep a uniform terminology for all the C_mH_m species, we call the short-bond forms Kekulé structures, labeled K_1^{cov} and K_2^{cov}, and construct from them the covalent state. Introduction of ionic mixing will be done by allowing the AOs of these structures to optimize freely and evolve into the CF AOs exemplified schematically in **4**.

Table 1 presents the energies required to distort (ΔE_{dis}) the C_mH_m molecules from D_{mh} to $D_{(1/2)mh}$. For each species we show the values for the covalent wavefunction with localized AOs, ΔE_{dis}(cov), and with CF orbitals, ΔE_{dis}(CF). Inspection of ΔE_{dis}(cov) values in entries 1a–3a shows that in all the cases the distortion energy is positive. This means that a pure singlet covalent state prefers a uniform geometry for all three molecules and even the antiaromatic covalent species prefer a uniform D_{mh} geometry. Entries 1b and 2b with the 6–31G basis set confirm that this behavior is physical and not an artifact of a small basis set. On the other hand, the ΔE_{dis}(CF) value remains positive for benzene, but becomes negative for cyclobutadiene (CBD) and cyclooctatetraene (COT). Thus, unlike the situation with the pure covalent state, when ionic structures are included through the CF AOs, the familiar behavior of the aromatic and antiaromatic compounds with respect to bond alternation is restored. This highlights the conclusion that those are the ionic structures that shape the distortivity behavior of the delocalized states of these species, and hence their tendency to undergo bond-localization or remain delocalized.

Table 1. Distortion energies ΔE_{dis}^{a} (kcal mol^{-1}) (1 kcal = 4.184 kJ)

Entry[b]	Compound	ΔE_{dis}(cov)	ΔE_{dis} (CF)
1a	C_4H_4	2.2	−2.6
1b		1.2	−2.6
2a	C_6H_6	3.3	3.0
2b		3.6	4.0
3a	C_8H_8	2.3	−5.8

[a] Calculated as the difference between the energy at the bond-alternated geometry and the uniform geometry, $\Delta E_{dis} = E[D_{(1/2)mh}] - E(D_{mh})$.
[b] In each entry, a stands for calculations with STO-3G basis set, and b for calculations with 6–31G basis set.

Which ionic structures are important? To achieve a more specific understanding of the role of ionicity, a detailed analysis of the ionic structures is required. The ionic structures form different ranks of ionicity by successive electron transfers from one site to the other; mono-ionics have a single ion pair, di-ionics have two, etc. In addition, the ionic structures have also covalent electron pairs across the non-ionic sites. For example, Scheme 3 shows the four ionic types for CBD, which make together 18 ionic structures; 12 of them are mono-ionic and 6 di-ionic. Benzene (for consideration of ionicity in aromatic and other delocalized species, see Ref. 29) and COT possess 60 and 280 mono-ionic structures, respectively, and so on.

In the first step, one needs to know whether all the ionic structures are indeed necessary to be considered for qualitative purposes. Table 2 shows the stabilization

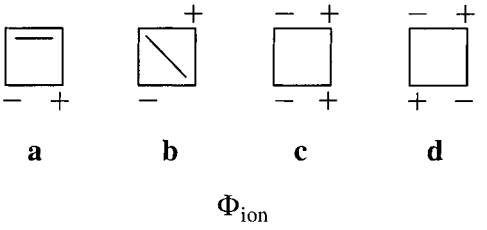

Scheme 3. Ionic structure types for CBD

Table 2. Stabilization energies (in kcal mol^{-1}), showing the effect of ionic structures

Entry	Compound	Basis set	E_{stab}(CF)	E_{stab}(ionic)	E_{stab}(mono-ionic)
1	CBD	STO-3G	52.7	52.7	51.8
2	Benzene		153.4	157.7	132.9
3	CBD	6–31G	26.7	20.0	19.9
4	Benzene		92.64	84.41	75.2

energies of the pure covalent state due to mixing of the ionic structures, for benzene and CBD. The first column shows the stabilization energy when all ionic structures are included via the CF orbitals, E_{stab}(CF). The second column, E_{stab}(ionic), lists the stabilization calculated from explicit covalent–ionic mixing calculations using localized AOs. The third column shows the same quantity when only mono-ionic structures are considered, E_{stab} (mono-ionic). Comparison of the different stabilization energies shows that the mono-ionic configurations are responsible for more than 95% and 80% of the total stabilization in CBD and benzene, respectively. [The 6–31G result that $E_{stab}(CF) > E_{stab}(ionic)$ arises because the explicit covalent–ionic calculations involve VB–CI without orbital optimization. The CF calculations involve orbital optimization and give a lower energy and higher E_{stab}. For the minimal basis set this does not create a disparity since orbital optimization lacks the degrees of freedom that larger basis set has.] It is reasonable to expect that a qualitative understanding of the role of covalent–ionic mixing can be derived by the consideration of the mono-ionic structures alone.

Factors controlling the covalent–ionic mixing.

Figure 1 shows a symmetry analysis of the covalent Kekulé structures for aromatic and antiaromatic species using benzene and CBD as the prototypes. The ground state for aromatics is always the positive combination, which transforms also as the totally symmetric representation in the D_{mh} point group.[10] On the other hand, the ground state for antiaromatic species transforms as the B_{1g} representation and involves the negative combination of their Kekulé structures.[10,12,27b,30–32] In the next section, we discuss the underlying reasons for the different ground-state combinations in the two classes, while at the moment we make use of the symmetry information to discuss the covalent–ionic mixing.

The 60 mono-ionic structures of benzene fall into groups which are distinguished by the distance between

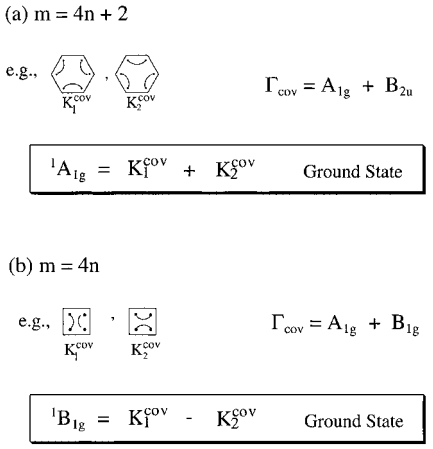

Figure 1. Symmetry analysis of the covalent states for (a) aromatic species, exemplified by benzene, and (b) antiaromatic species, exemplified by cyclobutadiene

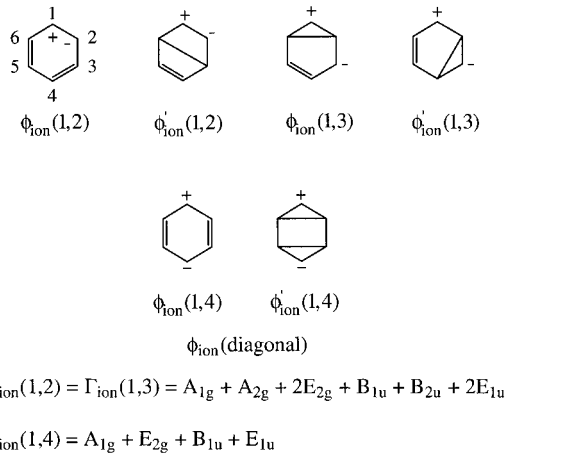

Figure 2. Mono-ionic structure types for benzene and their reducible symmetry representations

the ionic centers as shown in Fig. 2. The *ortho*-ionic structures are labeled $\Phi_{ion}(1,2)$, the *meta*-ionic as $\Phi_{ion}(1,3)$, and the *para*-ionic as $\Phi_{ion}(1,4)$. For uniformity with other species, the last type will also be called diagonal-ionic structures, Φ_{ion}(diagonal). Symmetry classification of these structures show that each type of the ionic structures has an A_{1g} combination with the appropriate symmetry to mix into the ground-state combination of the covalent Kekulé structures. To ascertain that this is also the case for higher ionicity, we analyzed also the di-ionic and tri-ionic structures, and once again each type contains A_{1g} combinations. In total, the entire set of 170 ionic structures of benzene contains 20 A_{1g} ionic combinations spanning all ranks and types of ionicity, which are able to mix into the covalent state combination of the Kekulé structures, described in Fig. 1. Explicit VB calculations showed that indeed *all* of these ionic types mix into the ground state.

Figure 3 shows a symmetry analysis of mono-ionic structural types for CBD. It is seen that the 1,2-ionic structures contain a B_{1g} combination, which can mix into the ground-state combination of the covalent state. In contrast, the diagonal-ionic structures do not contain any B_{1g} combination to mix into the covalent ground state. Thus, the diagonal-ionics are excluded by symmetry from mixing into the ground state of cyclobutadiene in the D_{4h} uniform geometry. A similar exclusion appears in the

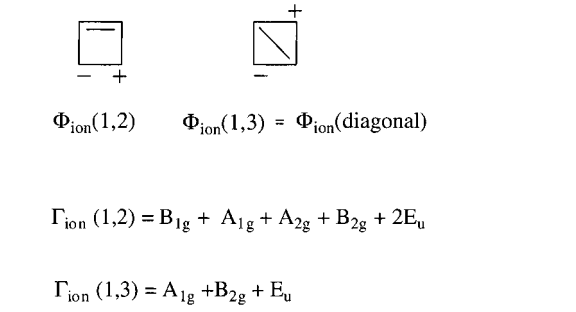

Figure 3. Mono-ionic structure types for cyclobutadiene and their reducible symmetry representations

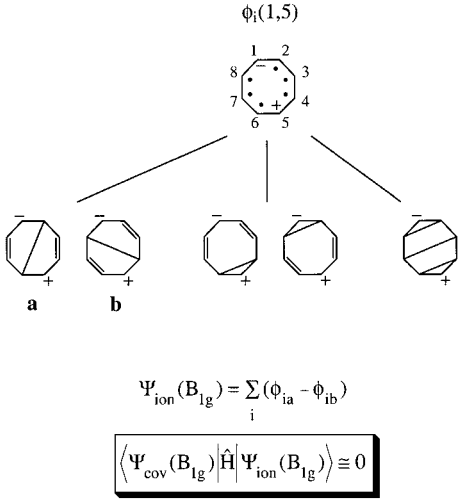

Figure 4. Diagonal-ionic structure types (with 1,5-ionicity) for cyclooctatetraene. The B_{1g} combination is made from structures **a** and **b**, and its matrix element with the covalent state is virtually zero. Note that the reduced resonance interaction ought to be written as in Eqn (6), $\beta_r = H_{ij} - E_i S_{ij}$, , but for convenience we show here and in Fig. 5 only the H_{ij} part

di-ionic structures as may be witnessed from the complete symmetry analysis in the supplementary material (available at the epoc website at http://www.wiley.com/epoc). It follows therefore, that although both benzene and square CBD are bond delocalized, their extent of electronic delocalization, in their uniform geometries, is different at the level of covalent–ionic mixing.

Much like in CBD, analysis of all 280 mono-ionic structures of COT shows that the diagonal-ionic structures are excluded from mixing into the covalent ground-state B_{1g} combination. Figure 4 shows how various types of diagonal-ionic structures can be constructed from a given 1,5-ion pair, $\Phi_i(1,5)$, by pairing the remaining six electrons into the possible five Rumer structures[28] available to the three pairs made from six odd electrons. Since there are eight possibilities to locate the 1,5-ion pair and each possibility gives rise to five structures, there are a total of 40 diagonal mono-ionic structures; 24 of these diagonal structures are excluded by symmetry from the covalent state. The other 16 structures form a B_{1g} combination that is made from the eight pairs of structures designated as Φ_{ia} and Φ_{ib}, which possess a 1,5-long bond and two short bonds. One might think that the ionic combination, $\Psi_{ion}(B_{1g})$, will mix strongly with the covalent $\Psi_{cov}(B_{1g})$ combination. However, our detailed VB calculations show that the ionic $\Psi_{ion}(B_{1g})$ combination virtually does not mix into the corresponding $\Psi_{cov}(B_{1g})$ combination of the covalent Kekulé structures; the mixing coefficients of these ionic structures are of the order of 0.0002, and their weight in the B_{1g} wavefunction of the ground state is virtually zero. This is expressed at the bottom of Fig. 4 by showing that the reduced resonance integral between the covalent and diagonal-ionic B_{1g} combinations is nearly zero. This exclusion reflects that the $\Psi_{cov}(B_{1g})$ covalent state is the negative combination of the Kekulé structures. Indeed, 1,5 diagonal structures of the types **a** and **b** (Fig. 4) possess virtually the same reduced resonance integral with either of the two covalent Kekulé structures. Since these Kekulé structures are combined in the covalent state with a negative sign, the individual reduced matrix elements of the **a** and **b** types diagonal-ionic structures with the covalent structures are practically zero. Thus, while 24 of the diagonal-ionics in Fig. 4 are excluded since they lack the B_{1g} symmetry, the other 16 structures, made from the $\Phi_{ia} - \Phi_{ib}$ combinations, are excluded owing to the 'node' in the covalent state, which is prompted by the negative combination of the Kekulé structures.

This is an important finding since the exclusion of the ionic–covalent mixing is an outcome of the 'node' in the covalent state and not of the strict spatial symmetry of the wavefunction. Let us briefly discuss this feature of the VB wavefunction that transcends spatial symmetry as described in a recent publication.[32b] Thus, as we shift the double bonds in one of the Kekulé structures, we generate the other one, but with a sign that depends on the number of π-bonds that are being switched in the cycle. This, in turn, determines the sign of the wavefunction for the ground state.[32b] If the cyclic switch generates the second Kekulé structure with a positive sign, the covalent state will be the positive combination of the Kekulé structures, and vice versa if the switch generates the negatively signed second Kekulé structure. This property can be defined as the electron-switch symmetry index (s) of the covalent-state, $s = (-1)^{N-1}$, N being the number of electron pairs in the π-system. For an aromatic species, the s index is positive, hence the covalent state is a positive combination of the Kekulé structures, and will mix all the ionic structures into the ground-state wavefunction. In contrast, antiaromatic species have a negative s and their covalent state will be the negative combination of the Kekulé structures, which thereby excludes the mixing of the diagonal ionic structures into the wavefunction. These trends are independent of the geometry or spatial symmetry, and this was verified by calculating CBD in D_{2h} symmetry ($R_1CC = 1.40$ Å, $R_2CC = 1.50$ Å). In this geometry, the all-positive combination of the diagonal ionic structures has the same spatial symmetry as the covalent state (both being A_g). Despite the identical spatial symmetry, the mixing of the diagonal ionic structures still obeys the electron-switch symmetry index and remains negligible (mixing coefficients are <0.002). This, in turn, means that allowance of the diagonal ionic structures into, or their exclusion from, the ground state is decided primarily by the electron-switch symmetry index irrespective of the geometry or spatial symmetry of the species, even though occasionally the electron-switch symmetry index and the spatial symmetry of the electronic structure might coincide.

We recall that electronic delocalization in a bond is in essence a measure of the extent of mixing of ionic

structures into the covalent state. As such, in aromatic situations such as benzene, where all possible ionic configurations mix into the covalent state, the state approaches perfect delocalization. However, in antiaromatic species such as CBD and COT, the diagonal-ionic structures are excluded from the ground-state wavefunction by the electron-switch symmetry index, leading therefore to imperfect delocalization. Thus, even though the electron density is uniformly distributed in the D_{nh} symmetry of all species (see also the vertical resonance energies in Scheme 1), the electronic delocalization in antiaromatics is impaired by the exclusion of the set of diagonal ionic structures. These mixing patterns are independent of spatial symmetry but they depend on the number of delocalized electron pairs. As such, they will persist to a large extent even in distorted geometries. It will be immediately seen that this exclusion is at the root of the different magnetic properties of the two classes of delocalized species.

The nature of the covalent state: Kekulé structures and spin-alternant states

Delving deeper into the fundamental building blocks of the wavefunction requires analysis of the electronic arrangements that make up the covalent state. Since these elements have been known for some time owing to studies by Mulder and Oosterhoff,[33] Kuwajima,[34] Maynau and Malrieu,[35] Shaik and co-workers,[36] Hiberty,[30] Zilberg and Haas,[31] Wu *et al.*,[32b] Klein *et al.*,[37] etc., we shall address the topic only briefly. The wavefunction of a Kekulé structure with $2N$ π-electrons is made of N pairs of covalent π-bonds. Such a covalent-pair wavefunction, called also the Heitler–London (HL) wavefunction, already appeared above in **1** for the H_2 bond.[38] In a many-electron system, the covalent wavefunction is the product of all the electron-pair wavefunctions. Thus, designating the p_π AOs in the cycle as 1, 2, ..., $2N$, as in drawing **5**, the covalent wavefunction for the 1–2 bond is given in Eqn (1a) as the corresponding determinantal wavefunction expressed with diagonal terms. Here, AOs with bars designate spin-down electrons and unbarred AOs indicate spin-up electrons. Each covalent Kekulé structure can, in turn, be written as a product of the HL wavefunctions of all the π-bonded pairs in the structure. Thus, the first Kekulé structure pairs are 1–2, 3–4, ..., $(2N-1)-(2N)$ as expressed in Eqn (1b), while the second Kekulé structure pairs are 2–3, 4–5, ..., $(2N)-1$, as in Eqn (1c) [normalization constants are dropped in Eqns (1a–c)].

$$b_{12} = |(1\bar{2}\text{–}\bar{1}2)| \tag{1a}$$

$$K_1^{\text{cov}} = \left|(1\bar{2}\text{–}\bar{1}2)(3\bar{4}\text{–}\bar{3}4)\cdots((2N-1)\overline{2N} - \overline{(2N-1)}2N)\right| \tag{1b}$$

$$K_2^{\text{cov}} = \left|(2\bar{3}-\bar{2}3)\cdots((2N-2)\overline{(2N-1)} - \overline{(2N-2)}(2N-1))((2N)\bar{1}-1\overline{(2N)})\right| \tag{1c}$$

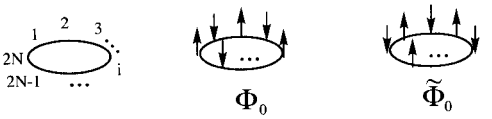

5 **6** **7**

Expanding the Kekulé structure wavefunctions results in a linear combination of 2^N determinants, which describe different patterns of arranging N p_π electrons with spin-up and N with spin-down in the $2N$ AOs. Each Kekulé structure contains 2^N such determinants with equal coefficients except for their signs as shown in Eqns 2(a) and (b):

$$K_1^{\text{cov}} = (\Phi_0 + (-1)^N\tilde{\Phi}_0) + \sum_{i=1}^{2^{N-1}} \pm\Phi_i' \tag{2a}$$

$$K_2^{\text{cov}} = (-1)^{N-1}\left[(\Phi_0 + (-1)^N\tilde{\Phi}_0) + \sum_{i=1}^{2^{N-1}} \pm\Phi_i''\right] \tag{2b}$$

Two of the determinants, labeled Φ_0 and $\tilde{\Phi}_0$ are unique relative to the rest. In these determinants, which are depicted in **6** and **7**, the electrons are arranged in an alternant manner, spin-up/spin-down, etc. These determinants, whose wavefunctions are given in Eqns 3(a) and (b), were earlier called the antiferromagnetic determinants, the Neel state[35] or the quasi-classical state[39] {note that the spin-alternant state is not a spin eigenfunction of the S^2 operator. As a rule, if one combination [e.g. Eqn (4a) or (4b)] gives rise to the ground singlet state, the opposite combination [e.g. $(\Phi_0 - \tilde{\Phi}_0)$, viz. the positive combination in Eqn (4a)] will generate the first excited triplet state[39c]}. Hereafter, they are referred to as the spin-alternant determinants.

$$\Phi_0 = |1\bar{2}3\bar{4}\cdots(2N-1)\overline{2N}| \tag{3a}$$

$$\tilde{\Phi}_0 = \left|\bar{1}2\bar{3}4\cdots\overline{(2N-1)}2N\right| \tag{3b}$$

The spin-alternant determinants represent the lowest energy arrangements of the spin system. All the other determinants represent spin arrangement patterns that are destabilized by Pauli repulsion among adjacent electrons with identical spins.[36b,39a] Φ_0 and $\tilde{\Phi}_0$ are the only determinants that are common to the two Kekulé structures. As can be seen from Eqns 2(a) and (b), the Φ_0–$\tilde{\Phi}_0$ combination is signed by $(-1)^N$, N being the number of electron pairs. As pointed out previously,[30] the sign of the combination can be deduced from Eqns 1(b) and (c). For example, Φ_0 is the product of all the first terms in each parenthetical expression in K_1^{cov}, Eqn 1(b), whereas $\tilde{\Phi}_0$ is the product of all the second terms in each parenthetical

expression in the equation. Hence, whereas the coefficients of the first terms are all positive leading to a positive coefficient of Φ_0, the coefficients of the second term are all negative (-1) and, therefore, the sign of $\tilde{\Phi}_0$ depends on N, the number of pairs of electrons, and is given as $(-1)^N$. Thus, as shown in Eqns 4(a) and (b), a spin-alternant state, Ψ_{sa}, with positive combination will typify the Kekulé structure of an antiaromatic cycle, while a negative combination will appear in the Kekulé structure of an aromatic situation.[39c]

$$\Psi_{sa}^{+}(2N = 4n) = \left(\Phi_0 + \tilde{\Phi}_0\right) \tag{4a}$$

$$\Psi_{sa}^{-}(2N = 4n + 2) = \left(\Phi_0 - \tilde{\Phi}_0\right) \tag{4b}$$

These combinations are depicted in **8** and **9** for benzene and CBD.

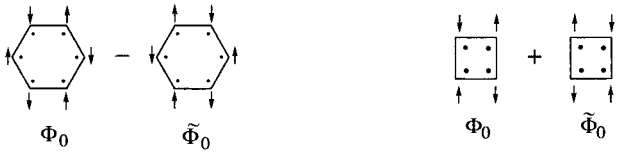

8 **9**

Symmetry properties of the spin-alternant-state. Since Φ_0 and $\tilde{\Phi}_0$ are the electron arrangements with the lowest energy, as was explained before,[30] it follows as a rule that the ground-state combination of the Kekulé structures, i.e. the covalent state, will be the one that retains the spin-alternant determinants, in contrast to the excited state combination which annihilates them. Based on Eqns 2(a) and (b), the sign of the covalent state combination depends, therefore, on the number of π-electron pairs N: negative $(K_1^{cov} - K_2^{cov})$ for $N = 2n$ and positive $(K_1^{cov} + K_2^{cov})$ for $N = 2n + 1$. In each case, the opposite Kekulé combination will have no contribution from the spin-alternant determinants and will generate an excited state, e.g. the $^1B_{2u}$ excited state of benzene.[30,32] Already at the level of the covalent state, made from the two Kekulé structures, the coefficients of the spin-alternant determinants are doubled relative to all other spin arrangement determinants. Adding all other Rumer[28] structures further increases the weight of these determinants in the wavefunction at the expense of the rest of the spin arrangements, which are destabilized by Pauli repulsions.[35,36,39a,c]

A symmetry analysis of the spin-alternant states for aromatics and antiaromatics is shown in Eqns 5(a) and (b):

$$(2N = 4n + 2);\ \Gamma(\Psi_{sa}^{-}) = A_{1g} \tag{5a}$$

$$(2N = 4n);\ \Gamma(\Psi_{sa}^{+}) = B_{1g} \tag{5b}$$

The opposite combinations of the spin-alternant determinants,[39c] in each case, have symmetries of higher excited states; for $4n + 2$, $\Gamma(\Psi_{sa}^{+}) = B_{1u}$, whereas for $4n$, $\Gamma(\Psi_{sa}^{-}) = A_{2g}$. Clearly, the spin-alternant states of aromatics and antiaromatics have the same symmetry as the ground states for aromatic (A_{1g}) and antiaromatic (B_{1g}) species, in the uniform geometries.[10,30,31] Thus, a very fundamental and natural reason is responsible for the ground state's spatial symmetries of these two classes. These symmetries are set by the spin-alternant state, which is the leading term of the ground-state wavefunction.

Molecules which possess no spatial symmetry follow the same rule, and can be classified by the electron-switch symmetry index, $s = (-1)^{N-1}$, N being the number of electron pairs (see above). For $N = 2n + 1$, the electron-switch symmetry index s is positive; hence the ground state is the positive combination of the Kekulé structures, and vice versa for $N = 2n$. These ground-state combinations of the Kekulé structures are the ones that retain the spin-alternant state. It follows, therefore, that the electron-switch symmetry index of the covalent state is also determined by the spin-alternant state. Since the spin-alternant state plays an important role in the ground-state wavefunction,[39c] our discussion follows with this state.

Covalent–ionic mixing of the spin-alternant states: a model for collective circulation of π-electrons

Simple inspection of the spin-alternant determinants in **6** and **7** reveals that the passage from one situation to the other is associated with a collective circular flow of the electrons and can, therefore, possibly model ring current, as has been conjectured and put to use in previous semiempirical VB studies.[34,35] What might possibly be the difference in this sense between aromatic and antiaromatic species? And how is all this connected with the magnetic properties of the two classes?

We can think of the collective circular mode as a resonance or mixing of the two spin-alternant determinants, as depicted in Fig. 5 for benzene and cyclobuta-

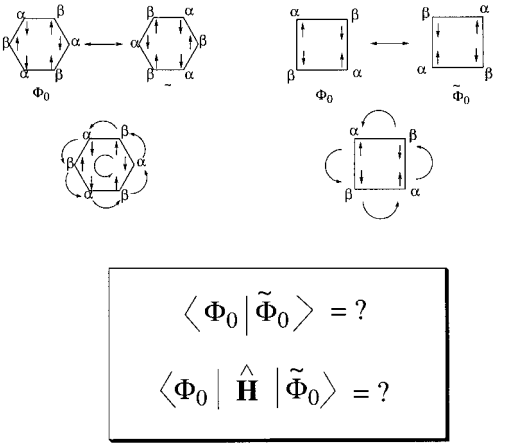

Figure 5. The reduced resonance between the spin-alternant determinants describes a collective circular motion of the π-electrons. The propensity of this 'motion' depends on the overlap and matrix element of the determinants

diene. The 'probability' of passing from Φ_0 to $\tilde{\Phi}_0$ or vice versa, depends on the overlap and reduced matrix element between these determinants, β_r, in Eqn (6) (recall that in VB theory the effective matrix element that controls the VB mixing is the reduced resonance integral[36a]).

$$\beta_r = H_{\Phi_0,\tilde{\Phi}_0} - E_{\Phi_0} S_{\Phi_0,\tilde{\Phi}_0}; \quad S_{\Phi_0,\tilde{\Phi}_0} = <\Phi_0|\tilde{\Phi}_0> \qquad (6)$$

where $H_{\Phi_0,\tilde{\Phi}_0}$ and $S_{\Phi_0,\tilde{\Phi}_0}$ are the resonance and the overlap integrals between the two spin alternant determinants Φ_0 and $\tilde{\Phi}_0$ and E_{Φ_0} is their self-energy (both Φ_0 and $\tilde{\Phi}_0$ have the same energy).

These critical quantities were calculated with two orbital types in the determinants, viz. purely localized AOs and CF AOs. We recall that the latter AOs introduce effectively the ionic structures that are permitted by symmetry. The β_r values for Φ_0 and $\tilde{\Phi}_0$ along with the overlap values, *S*, between them are shown in Table 3.

The first trend in Table 3 is in the overlap integral, which is strictly zero for antiaromatics but is finite for aromatics. This information means that the collective circular motion in aromatics is sustained by the overlap of the p_π AOs. In contrast, overlap cannot sustain circulatory movement of the $4n$ electrons in antiaromatic situations. How do ionic structures affect these overlap considerations? Inspection of the overlaps based on CF AOs shows that incorporation of the ionic structures indeed intensifies the overlap in the aromatic situations, whereas in the antiaromatic situations the overlap remains strictly zero. The energetic aspect of the mixing of the spin-alternant determinants is provided by the β_r values in Table 3; these values follow the same trends as the overlaps. It is seen that with localized AOs, all β_r values are very small. In comparison, using CF AOs slightly increases the β_r values for antiaromatics, but not by much, leaving β_r(CF) a very small fraction of the total resonance energy of the antiaromatics (see Scheme 1). On the other hand, in the $4n+2$ aromatic cycles the β_r(CF) value increases significantly, and in the case of benzene it amounts to half of the entire vertical resonance energy (see Scheme 1). It is clear, therefore, that the circulatory motion, which is implicit in the resonating spin-alternant state, is much less effective with the pure covalent determinants and requires ionic structures to mediate this flow. Moreover, in the case of antiaromatic species, the ionic structures do not seem to be very helpful in mediating the circulatory motion of the electrons. These trends are in line with the conclusions drawn about delocalization, in the previous section, and which show that in antiaromatic species, a set of diagonal-ionic structures is excluded from mixing into the delocalized state of an antiaromatic cycle, as opposed to complete ionic mixing in the case of the aromatic cycles. Since the spin-alternant state determines the symmetry features of the ground state for aromatic and antiaromatic species, it follows that the ionic–covalent mixing at the level of the spin-alternant state controls the overall covalent–ionic mixing in the ground state.

It is apparent that the mixing of the spin-alternant determinants and the delocalization of the complete electronic states exhibit the same trends with respect to the importance of the ionic structures. Both properties require assistance of the ionic structures, and this assistance depends on the parity of the electron-switch symmetry index which distinguishes the aromatic and antiaromatic situations. Therefore, we may represent these trends in a single pictorial manner based on the spin-alternant determinants. Scheme 4 depicts a representation of the 'electron flow' in terms of the $\Phi_0 \leftrightarrow \tilde{\Phi}_0$ interchange mediated by ionic structures generated by one-electron transfer (mono-ionics) from an α-spin site to a β-spin site and vice versa. In (i), we show the situation in benzene where starting from Φ_0 and following the arrows, the interchange to $\tilde{\Phi}_0$ is mediated via a procession of ionic situations **a**–**e**. [Note that the ionic structures belong to the two Kekulé structures, and hence the description in Scheme 4 refers to the situation in the full state, not to a single Kekulé structure as might have been deduced from Eqns (2a) and (2b). Any carbon could serve as a starting point in Scheme 4. Hence the first electron transfer can result with spin arrangement relating to anyone of the different *ortho*-dipolar ionic structures; the second, with spin arrangement relating to anyone of the different *meta*-dipolar ionic structures etc.] Therefore, in a static sense, the electron flow and delocalization around the circumference of the ring suffers no interruption. The case of CBD is shown in (ii), where the interchange of Φ_0 and $\tilde{\Phi}_0$ cannot be mediated by the ionic situations and the circular flow is frustrated due to

Table 3. Reduced resonance integral[a] between the two spin alternant determinants in kcal mol^{-1}

Entry[b]	Compound	*S*(localized)	*S*(CF)	β_r(localized)	β_r(CF)
1a	C_4H_4	0.000	0.000	0.2	0.8
1b	C_4H_4	0.000	0.000	0.6	1.3
2a	C_6H_6	0.000	0.122	0.7	33.9
2b	C_6H_6	0.005	0.165	4.4	38.3
3a	C_8H_8	0.000	0.000	0.0	0.2
4a	$C_{10}H_{10}$	0.000	0.023	0.04	9.6

[a] Eqn (6).
[b] In each entry, a refers to STO-3G results and b to 6–31G results.

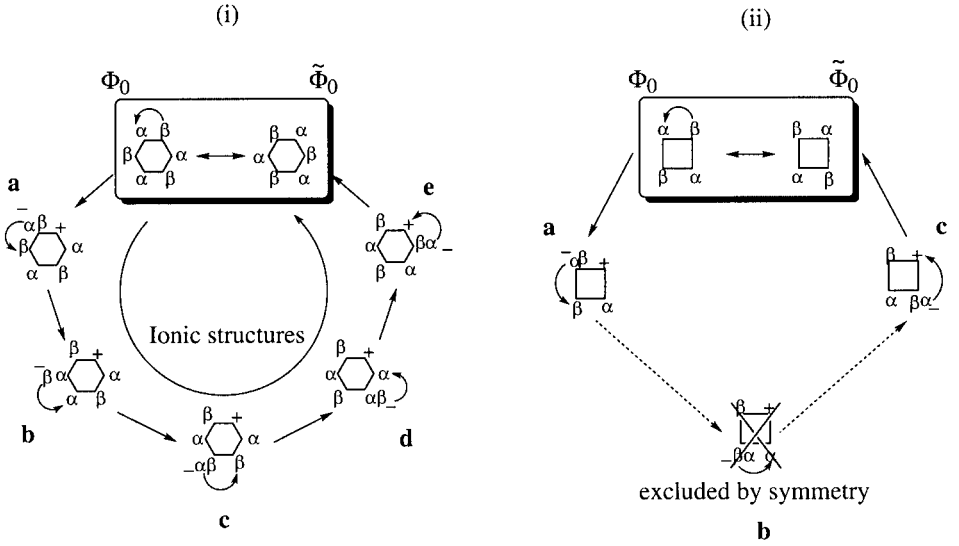

Scheme 4. Interchange diagrams for the spin alternant determinants. (i) In benzene the flow is mediated by ionic situations **a**–**e**. (ii) In CBD the flow is interrupted due to exclusion of the diagonal-ionic situation **b**

the exclusion of the diagonally ionic situation **b**. The electron flow of the electrons around the C_4H_4 ring is, therefore, interrupted and imperfect delocalization sets in.

The two interchange diagrams in Scheme 4 are archetypal for aromatic and antiaromatic species C_mH_m ($m = 4n + 2$; $4n$) with an average of one π-electron per site, be they in their uniform or bond-alternated geometries.

The spin-alternant state and ring currents in $4n + 2$ and $4n$ systems

The probability of a collective circular flow of the electrons in the spin-alternant state can be used to draw a link between the mode of delocalization and the magnetic properties.[34,35] In view of the significance of the magnetic property,[2] which serves as a uniquely applicable criterion for characterizing aromaticity and antiaromaticity, establishing such a link is important.

Aromatic species are characterized by enhanced diamagnetism, whereas antiaromatics by exalted paramagnetism[2,40] (Λ values of -13.4 for benzene and $+12.5$ for CBD are given in Ref. 41, but in these sources CBD has a D_{2h} geometry). The diamagnetic/paramagnetic enhancement, Λ, of a compound is defined by the magnetic susceptibility exhibited by the compound, χ_{av}, relative to a localized model with susceptibility that obeys bond additivity, χ'_{av}:

$$\Lambda = \chi_{av} - \chi'_{av} \tag{7}$$

Table 4 presents the average magnetic susceptibility values, χ_{av}, its in-plane (χ_{ip}) and perpendicular (χ_{zz}) components, and the diamagnetic enhancement, Λ, for

Table 4. Magnetic susceptibilities and exaltations of CBD and benzene (in ppm csg)

Entry	Compound	Parameter	$\chi'^{a,b}_M$	χ^{cal}_M	$\chi^{exp c}_M$	$\Lambda^{d,e}$
1a	CBD	χ_{ip}	-30.0	-30.0^f		
1b		χ_{zz}	-45.1	$+17.7^f$		
1c		χ_{av}	-35.0 (-27.4)	-14.1^g		$+20.9$ ($+13.3$)
2a	Benzene	χ_{ip}	-45.1	-47.1^h	-34.9	
2b		χ_{zz}	-67.7	-109.6^h	-94.6	
2c		χ_{av}	-52.6 (-41.1)	-67.9^h	-54.8	-15.3 (-26.8)

[a] χ'_M values calculated according to the IGLO increment system from Ref. 7.
[b] The values in parentheses are calculated according to the Haberditzl increment system, Ref. 40b.
[c] Experimental data from Ref. 7.
[d] Exaltation values calculated as the difference between χ^{calc}_M and χ'_M according to the IGLO increment system, Ref. 7.
[e] The enhancement values in parentheses are calculated as the difference between χ^{calc}_M and χ'_M according to the Haberditzl increment system, Ref. 40b. Similar results were obtained by Schleyer and co-workers.[41]
[f] Estimated values following the assumption that $\chi^{calc}_{ip} \approx \chi'_{ip}$ concluded from Ref. 7.
[g] Calculated by the MC-IGLO method, Ref. 8.
[h] Calculated by the coupled Hartree–Fock method, Ref. 7.

both CBD and benzene (entries 1c and 2c). Some of the values were computed by Kutzelnigg and co-workers;[7,8] others were estimated using the calculated values and increment schemes. Two different increment schemes were used in order to calculate $\chi'_{\mathrm{av},}$[7,40b] resulting in different absolute values which reveal the same trend.[41] It is seen that whereas benzene exhibits diamagnetic enhancement, ($\Lambda < 0$), CBD has an oppositely signed or paramagnetic enhancement ($\Lambda > 0$). [$\chi_{\mathrm{av}}^{\mathrm{cal}}$ is not given at the same level of calculation for both molecules, yet comparison with the results obtained by Schleyer *et al*.[41] implies that this trend ($\Lambda < 0$ for benzene and $\Lambda > 0$ for CBD) is reliable; and since the interest of this paper is qualitative ideas, it is deemed sufficient.] Analysis of the in-plane and out-of-plane contributions to the magnetic susceptibility (entries 1a,b and 2a,b) shows that the oppositely signed enhancements of these species originate in the out-of-plane contributions (χ_{zz}).

Despite the controversy that had surrounded[6–8,14,15] the origins of the enhanced diamagnetism of aromatic compounds, in the direction perpendicular to the plane of the ring (χ_{zz}), the careful analysis of Kutzelnigg and co-workers[7] makes a good case for 'diamagnetic ring currents.' Thus, the diamagnetic ring current should be associated with a collective 'circulation' of the electrons across the perimeter of the aromatic ring. The result of this motion behaves in accord with the classical Lenz–Biot–Savar law and induces an internal magnetic field which opposes the external field.[42] To the best of our knowledge, a clear visual model that rationalizes the paramagnetic effect in antiaromatic species has not been given in a similar manner. Since we just argued that the circular motion is interrupted in antiaromatic species, we would like to inquire how, if at all, these magnetic effects could be associated with the intrinsic property of the π-system to sustain a circular π-flow. This can be discussed by considering the interchange diagrams in Scheme 4 under influence of an external magnetic field (placed in the direction perpendicular to the ring).

Thus, in the absence of magnetic field, the two directions of the electron flow in Scheme 4 are degenerate, and the stationary state is an interference of both directions. However, the application of an external magnetic field selects a preferred direction of motion in a manner that creates an opposing internal magnetic field. In a quantum mechanical system, the electrons will flow around the ring's perimeter in the requisite direction only if all required ionic situations could mix and mediate a continuous flow that generates the diamagnetic ring current. Thus, benzene and other aromatic species are expected to have strong diamagnetic contribution due to ring current, since the electron flow is assisted by all possible ionic structures [(i), Scheme 4]. One might say that in aromatic species the disposition for ring current exists already in the electronic structure of the ground state. In contrast, in CBD where the diagonal-ionic structures are excluded from the ground-state wavefunction, the flow of electrons is interrupted, and a diamagnetic ring current cannot be elicited.

While these considerations explain the excess diamagnetism of aromatics, they do not give a clue as to the origins of the enhanced paramagnetism of antiaromatic compounds. Furthermore, the zero overlap and tiny destabilizing matrix element in the spin-alternant state of CBD (Table 3) suggest that a simple circulatory motion of the p_π electrons in a direction opposite to that of benzene is not likely to be a reasonable model for the observed paramagnetism. We must, therefore, probe this effect by going into the quantum chemical definition of magnetic susceptibility.

The magnetic susceptibility parameter, χ, consists of two oppositely signed contributions, a diamagnetic contribution χ^{d} and a van Vleck paramagnetic contribution χ^{p}, as shown in Eqn (8):[42]

$$\chi = \chi^{\mathrm{d}} + \chi^{\mathrm{p}} = -N_\chi^{\mathrm{d}}\langle 0|r^2|0\rangle + N_\chi^{\mathrm{p}} \sum_{n\neq 0} \frac{\langle 0|\hat{L}|n\rangle\langle n|\hat{L}|0\rangle}{E_n - E_0} \tag{8}$$

where $\hat{L}$ is the angular momentum operator of the electrons, r is the distance from the nucleus, $|0\rangle$ and $|n\rangle$ are the ground and excited states respectively, E_0 and E_n are their respective energies and N_χ^{d} and N_χ^{p} are constants.[42] ($N_\chi^{\mathrm{d}} = N_0 e^2/4mc^2$ and $N_\chi^{\mathrm{p}} = N_0 e^2/2m^2c^2$, where e and m are, respectively, the charge and mass of the electron, c is the speed of light and N_0 is Avogadro's number). Similar equations with a weighing factor of $1/r^3$ describe the chemical shift property. Equation (8), which is appropriate for cases with no state degeneracy and where orbitals are represented only by real wavefunctions, is applicable to benzene and CBD.[43] (One can form two imaginary combinations from the degenerate pair of CBD orbitals. The imaginary orbitals now look like the imaginary combinations of the p_x and p_y AOS which have angular momenta $M_{\mathrm{L}} = \pm 1$. Double occupation in any one of the combinations should in principle have angular momentum, and can possibly account for the paramagnetic ring currents. We thank W. T. Borden for discussing this point. This angular momentum state is precisely the B_{1g}–B_{2g} mixed state shown in Scheme 5. Our state representation can be shown to be equivalent.) The equation shows that whereas diamagnetism is an intrinsic property of the electronic structure in the ground state, paramagnetism arises owing to angular momentum generated by mixing of excited states into the ground state. The two contributions are oppositely signed and they reflect the different modes of interaction with the external magnetic field; diamagnetism leads to some destabilization and paramagnetism to stabilization.

A symmetry analysis of the terms may reveal qualitative trends in the relative contributions of the diamagnetic and paramagnetic terms for aromatics and antiaromatics. The diamagnetic term of the magnetic susceptibility, χ^{d},

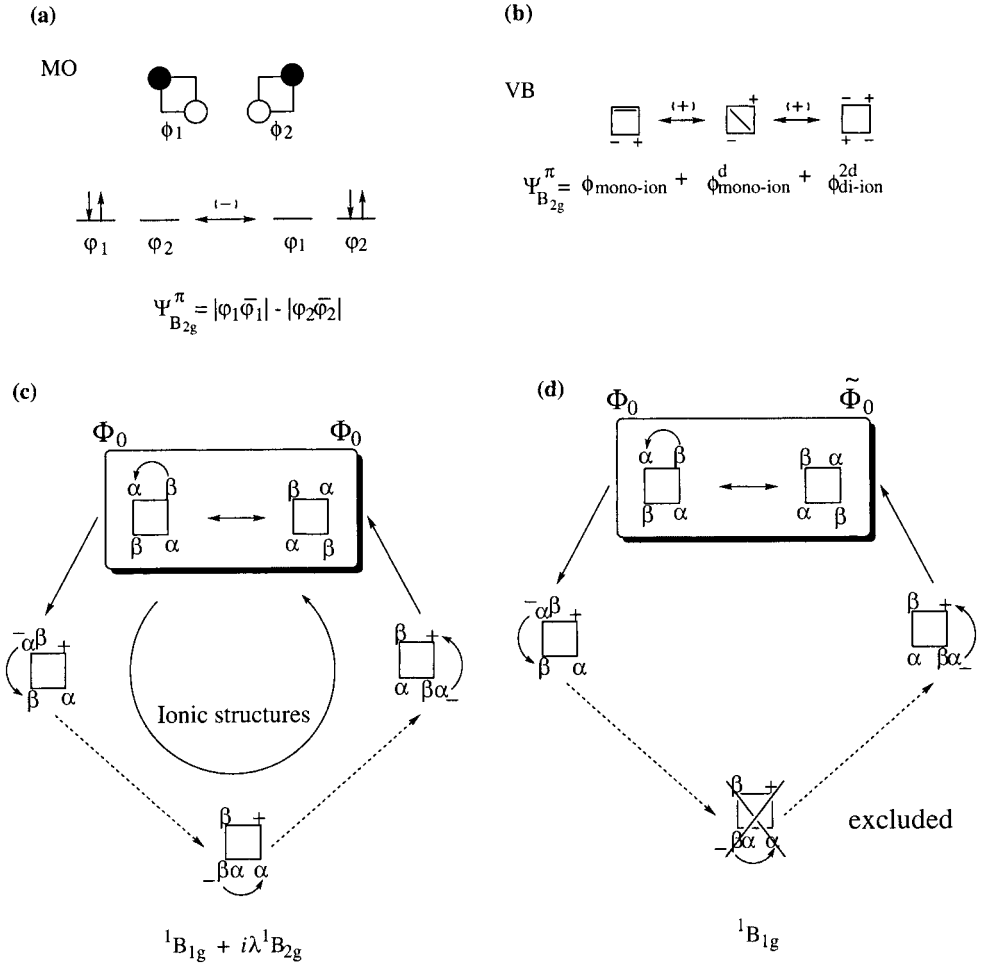

Scheme 5. π-MO occupancy, in (**a**), for the first $^1B_{2g}$ excited state of CBD, and the corresponding VB description in (**b**). The mixing of $^1B_{2g}$ provides the missing ionic structures to mediate the continuous π-flow. The diagrams in (**d**) and (**c**) contrast the excluded flow in the ground state, $^1B_{1g}$, viz. the continuous flow in the magnetic state

is a property of the ground-state wavefunction alone. It depends on the distance from the nucleus, r, which is a scalar and as such behaves as the totally symmetric representation, Γ_1, of the molecular point group. Therefore, based on symmetry considerations alone, the diamagnetic term should be non-zero in all cases since the direct product of any state's symmetry with itself always contains the totally symmetric representation. Both benzene and CBD would exhibit diamagnetic contribution to χ. However, benzene, whose ground-state wavefunction includes all of the ionic structures in a manner that permits electron circulation [Scheme 4 (i)], is expected to have a larger π-diamagnetic term compared with CBD, which lacks the diagonal ionic structures and hence cannot sustain π-electron circulation.

The paramagnetic term, on the other hand, depends on the angular momentum operator $\hat{L}$, which is the sum of the corresponding operators for the individual electrons. The expectation value with respect to each such mono-electronic operator is the sum of the expectation values of the Cartesian components. These Cartesian components have symmetry properties as the real rotations of the point group.[44,45] Therefore, a non-zero paramagnetic term in Eqn (8) requires that the direct product of the irreducible representations of the ground and excited states, $\Gamma(|0\rangle)$ and $\Gamma(|n\rangle)$, will be equal to the representation of the real rotations, $\Gamma(R_k)$, of the point group, as expressed in Eqn (9):

$$\chi^{\mathrm{p}} \neq 0;\ \Rightarrow\ \Gamma(|0\rangle) \otimes \Gamma(|n\rangle) = \Gamma(R_k) + \text{others} \qquad k = x, y, z \tag{9}$$

Furthermore, Eqn (8) shows that the paramagnetic contribution is inversely proportional to the energy gap between the ground state and the excited states, which through mixing induce the paramagnetic effect. Thus, significant contributions are expected mostly from the low-lying excited states that possess the requisite symmetry to mix efficiently with the ground state in the external magnetic field, and to elicit thereby angular momentum in the combination state.

With the above guidelines, we now seek appropriate low-lying excited states for CBD. Following the symme-

try rule in Eqn (9), the z component of the paramagnetic susceptibility will be contributed by mixing excited states of B_{2g} symmetry, into the B_{1g} ground state, while x, y components require excited states of E_g symmetry. For comparison, paramagnetic effects for benzene are induced by excited states of A_{2g} symmetry (for z contribution) and E_{1g} symmetry (for x, y contributions).

We must focus on the z component, which makes the difference between the two classes (Table 4). According to MRCCSD(T) results by Balková and Bartlett,[46] the B_{2g} excited state of CBD lies only 2.28 eV above the ground state in the square geometry. In contrast, the lowest A_{2g} excited state for benzene lies more than 6.2 eV above the ground state and is a Rydberg state, according to the CASPT2 calculations of Roos and co-workers.[47] The availability of a low-lying excited state with the appropriate symmetry for CBD and not for benzene seems sufficient to account for the higher paramagnetism of CBD. However, one still wonders how the $B_{2g} \rightarrow B_{1g}$ mixing can actually result in a circulatory motion of the π-electrons in CBD, a motion otherwise interrupted by the excluded diagonal-ionic structures?

The lowest excited states of CBD are those that involve excitation within the π-frame. Scheme 5 shows that the second lowest Ψ^{π} excited state (S_2) of CBD is $^1\Psi^{\pi}_{B_{2g}}$ which, according to the symmetry analysis, has the appropriate symmetry to mix into the B_{1g} ground state and induce a paramagnetic z-directed contribution to χ^{p}. Now, in the presence of the magnetic field, the wavefunction of CBD will be given by the linear combination in Eqn (10), with the real part being the original B_{1g} state, and an imaginary part given by the B_{2g} component:

$$\Psi(C_4H_4) = \Psi_{B_{1g}} + i\lambda\Psi^{\pi}_{B_{2g}} \qquad (10)$$

where λ = mixing coefficient. Expansion of the $\Psi^{\pi}_{B_{2g}}$ state into VB structures shows (see **b** in Scheme 5) that this state contains the missing diagonal-ionic structures, which are excluded in the ground-state wavefunction. Hence the magnetic field induced-mixing of $\Psi^{\pi}_{B_{2g}}$ into the ground-state $\Psi_{B_{1g}}$ provides precisely those requisite ionic structures that now permit a circular flow of the π-electrons. The interchange diagram in **c** in Scheme 5 contrasts this continuous flow in the presence of the magnetic field with the interrupted flow in the ground state in **d**. In other words, the magnetically induced B_{1g}–B_{2g} mixing generates angular momentum, and hence a paramagnetic ring current can interact favorably with the external field. Owing to its paramagnetic origins [Eqn (8)], this circular motion leads to an oppositely signed magnetic moment compared with the diamagnetic term of benzene that arises due to the circular π-flow in the ground-state wavefunction (Scheme 4).

In summation, in aromatic species the ground-state electronic structure is disposed for ring current due to π-electron circulation. In the presence of an external magnetic field this disposition for circulation chooses a direction that leads to a diamagnetic effect responsible for the enhanced diamagnetism of the molecule. By contrast, the ground electronic state of antiaromatic species cannot sustain a π-electron ring current due to the exclusion of diagonal ionic structures that have to mediate this circulation. However, the mixing of $^1B_{2g}$ excited state into the $^1B_{1g}$ ground state in the presence of the external field provides the excluded ionic structures and enables a circulatory π-electron flow. This flow generates angular momentum, and hence paramagnetic ring currents, which are responsible for the enhanced paramagnetism of the species.

CONCLUSIONS

A detailed description of aromatic and antiaromatic systems was given from a VB theoretical perspective. In VB terms, electron delocalization is a result of the mixture of ionic and covalent configurations (see **1**–**3**). Perfect delocalization is referred to situations where *all* ionic configurations mix with the covalent state and contribute equally to the electronic structure. An imperfect delocalization occurs whenever a set of ionic structures is excluded from mixing by spatial or permutation symmetry. Our analysis shows that aromatic species are typified by perfect delocalization, whereas antiaromatic species by imperfect delocalization due to the exclusion of diagonal-ionic structures in the ground state.

These features and the magnetic properties of aromatic and antiaromatic species can be traced to the properties of the spin-alternant state that constitutes the dominant component of the two Kekulé structures. The spin-alternant state is a mixture of the two possible electron arrangement patterns that alternate the electronic spin around the perimeter of the ring. The interference of the spin-alternant determinants in the spin-alternant state (Fig. 5) describes a collective circular motion of the electrons along the perimeter of the ring. The overlap and matrix element of these determinants is a measure of the probability of this collective flow. In this sense, the aromatic situations are typified by a significant overlap and matrix element, both of which are intensified when the ionic structures are included. By contrast, in antiaromatic species, the overlap is zero and the matrix element is very small. Furthermore, none of these properties of antiaromatics are affected significantly by allowing the ionic structures to mix in. Thus, as shown in Scheme 4, the circular electron flow in aromatic species exists already in the ground state, whereas in antiaromatic species this collective motion is interrupted due to the exclusion of the diagonal-ionic structures. This exclusion of ionic structures is driven by the electron-switch symmetry index of the wavefunction, defined by $s = (-1)^{N-1}$, N being the number of π-electron pairs, and hence are

general for aromatic and antiaromatic species irrespective of geometry or spatial symmetry.

In the presence of a magnetic field, the circular π-motion in the aromatic spin-alternant state selects a preferred direction that results in an exalted diamagnetism in the direction perpendicular to the molecular plane. By contrast, in antiaromatic species, the diagonal ionic structures, which are required to complete the circular π-electron flow, are brought in only via admixture of the $^1B_{2g}$ excited states due to the external magnetic field. This mixing allows π-circulation and creates van Vleck paramagnetism.

The predictive power of this model will have to be further tested, for example, to explain the unusual inversion of the magnetic properties reported by Schleyer and co-workers[41] for the triplet states of $4n$ and $4n+2$ species. Our initial analysis shows that the symmetry conditions are met for such an inversion in the case of $4n$ species.

Acknowledgments

Illuminating discussions with Professors W. T. Borden and Ch. Van Wüllen and Drs M. Filatov and T. Müller are acknowledged. The research at the Hebrew University was supported in part by a Niedersachsen grant given by the Ministry of Science and Culture of the State of Niedersachsen, and in part by a Robert Szold grant.

REFERENCES

1. (a) Minkin VI, Glukhovtsev MN, Simkin BYa. *Aromaticity and Antiaromaticity, Electronic and Structural Aspects*. Wiley: New York, 1994; (b) Bergmann ED, Pullman B (eds). *Aromaticity, Pseudoaromaticity, Anti-aromaticity.* Symposium on Quantum Chemistry and Biochemistry. Israel Academy of Science and Humanities: Jerusalem, 1971, vol. **3**; (c) Lloyd D. *The Chemistry of Conjugated Cyclic Compounds. To Be or Not To Be Like Benzene?* Wiley: Chichester, 1989; (d) Gerratt PJ. *Aromaticity.* Wiley: New York, 1986; (e) Schleyer PvR (guest ed). *Chem. Rev.* 2001; **101**: 1115–1566; (f) Brush SG. *Stud. Hit. Philos. Sci*. 1999; **30**: 21; 1999; **30**: 263.
2. Schleyer P von R, Jiao H. *Pure Appl. Chem.* 1996; **68**: 209.
3. (a) Yu Z-H, Xuan Z-Q, Wang T-X, Yu H-M. *J. Phys. Chem. A* 2000; **104**: 1736; (b) Sawicka D, Houk KN. *J. Mol. Model.* 2000; **6**: 158; (c) Deniz AA, Peters KS, Snyder GJ. *Science* 1999; **286**: 1119; (d) Balawender R, Komorowski L, De Proft F, Geerlings P. *J. Phys. Chem. A* 1998; **102**: 9912; (e) Lloyd D. *J. Chem. Inf. Comput. Sci.* 1996; **36**: 442; (f) Cyranski MK, Krygowski TM, Katritzki AR, Schleyer PvR. *J. Org. Chem.* 2002; **67**: 1333.
4. (a) Hückel E. *Z. Phys.* 1930; **60**: 423; (b) Hückel E. *Z. Phys.* 1931; **72**: 310; (c) Hückel E. *Trans. Faraday Soc.* 1934; **30**: 40.
5. Bally T, Masamune S. *Tetrahedron* 1980; **36**: 343.
6. Gomes JANF, Mallion RB. *Chem. Rev.* 2001; **101**: 1349.
7. Fleischer U, Kutzelnigg W, Lazzeretti P, Mühlenkamp V. *J. Am. Chem. Soc.* 1994; **116**: 5298.
8. van Wüllen C, Kutzelnigg W. *Chem. Phys. Lett.* 1993; **205**: 563.
9. Matsuura A, Komatsu K. *J. Am. Chem. Soc.* 2001; **123**: 1768.
10. Shaik S, Shurki A, Danovich D, Hiberty PC. *Chem. Rev.* 2001; **101**: 1501.
11. Hornig DF. *J. Am. Chem. Soc.* 1950; **72**: 5772.
12. Voter AF, Goddard WA, III. *J. Am. Chem. Soc.* 1986; **108**: 2830.
13. McWeeny R. *Proc. Soc. Phys. London* 1953; **A66**: 714.
14. (a) London F. *J. Phys. Radium* 1937; **8**: 399; (b) Pople J A. *J. Chem. Phys.* 1956; **24**: 1111; (c) Schneider WG, Bernstein H, Pople JA. *J. Am. Chem. Soc.* 1958; **80**: 3497; (d) Pople JA. *Mol. Phys.* 1958; **1**: 175; (e) Haigh CW, Mallion RB. *Prog. Nucl. Magn. Reson. Spectrose*. 1980; **13**: 303; (f) Haddon RC, Haddon VR, Jackman LM. *Top. Curr. Chem.* 1970; **16**: 103; (g) Pople JA, Untch KG. *J. Am. Chem. Soc.* 1966; **88**: 4811.
15. (a) McWeeny R. *J. Chem. Phys.* 1949; **17**: 1341; *Mol. Phys.* 1958; **1**: 311; (b) Musher JI. *J. Chem. Phys.* 1965; **43**: 4081; 1967; **46**: 1219; (c) Musher JI. *Adv. Magn. Reson.* 1966; **2**: 177; (d) Lazzeretti P, Malagoli M, Zanasi R. *J. Mol. Struct.* (*THEOCHEM)* 1991; **234**: 127; (e) Lazzeretti P, Rossi E, Zanasi R. *J. Chem. Phys.* 1982; **77**: 3129; (f) Lazzeretti P, Zanasi R. *J. Chem. Phys.* 1981; **75**: 5019; *Chem. Phys. Lett.* 1983; **100**: 67; (g) Blustin PH. *Chem. Phys. Lett.* 1979; **64**: 507.
16. (a) Verbeek J, Langenberg JH, Byrman CP, Dijkstra F, Van Lenthe JH. *TURTLE—Ab Initio VB/VBSCF/VBCI Program*. Theoretical Chemistry Group, Debye Institute, University of Utrecht: Utrecht, 1993–2000; (b) van Lenthe JH, Dijksra F, Havenith WA. In *Valence Bond Theory*, Cooper DL (ed). Elsevier: Amsterdam, 2002; 79.
17. (a) Grein F, Chang TC. *Chem. Phys. Lett.* 1971; **12**: 44; (b) Banerjee A, Grein F. *Int. J. Quantum Chem.* 1976; **10**: 123.
18. Levy B, Berthier G. *Int. J. Quantum Chem.* 1968; **2**: 307.
19. Frisch MJ, Trucks GW, Schlegel HB, Gill PMW, Johnson BG, Robb MA, Cheeseman JR, Keith T, Petersson GA, Montgomery JA, Raghavachari K, Al-Laham MA, Zakrzewski VG, Ortiz JV, Foresman JB, Cioslowski J, Stefanov BB, Nanayakkara A, Challacombe M, Peng CY, Ayala PY, Chen W, Wong MW, Andres JL, Replogle ES, Gomperts R, Martin RL, Fox DJ, Binkley JS, Defrees DJ, Baker J, Stewart JP, Head-Gordon M, Gonzalez C, Pople JA. *Gaussian 94, Revision D.4*. Gaussian: Pittsburgh, PA, 1995.
20. Werner H-J, Knowles PJ, Amos RD, Bernhardsson A, Berning A, Celani P, Cooper DL, Deegan MJO, Dobbyn AJ, Eckert F, Hampel C, Hetzer G, Korona T, Lindh R, Lloyd AW, McNicholas SJ, Manby FR, Meyer W, Mura ME, Nicklass A, Palmieri P, Pitzer R, Rauhut G, Schütz M, Stoll H, Stone AJ, Tarroni R, Thorsteinsson T. *MOLPRO*. University of Birmingham, 1998.
21. (a) Werner H-J, Knowles PJ. *J. Chem. Phys.* 1985; **82**: 5053; Knowles PJ, Werner H-J. *Chem. Phys. Lett.* 1985; **115**: 259; (b) Knowles PJ, Werner H-J. *Theor. Chim. Acta* 1992; **84**: 95.
22. Coulson CA, Fischer I. *Philos. Mag.* 1949; **40**: 386.
23. (a) McWeeny R, Jorge FE. *J. Mol. Struct. (THEOCHEM)* 1988; **169**: 459; (b) Gallup GA. In *Valence Bond Theory*, Cooper DL (ed). Elsevier: Amsterdam, 2002; 1; (c) Wu W, Mo Y, Zhang Q. In *Valence Bond Theory*, Cooper DL (ed). Elsevier: Amsterdam, 2002; 143.
24. (a) Cooper DL, Gerratt J, Raimondi M. *Adv. Chem. Phys.* 1987; **69**: 319; (b) Gerratt J, Cooper DL, Raimondi M. *Int. Rev. Phys. Chem.* 1988; **7**: 59; (c) Gerratt J, Cooper DL, Raimondi M. In *Valence Bond Theory and Chemical Structure*, Klein DJ, Trinajstic N (eds). Elsevier: Amsterdam, 1990; 287; (d) Cooper DL, Gerratt J, Raimondi M. *Chem. Rev.* 1991; **91**: 929.
25. Bobrowicz FW, Goddard WA. In *Modern Theoretical Chemistry: Methods of Electronic Structure Theory*, vol. **3**, Schaefer HF (ed). Plenum: New York, 1977; 79.
26. (a) Cooper DL, Gerratt J, Raimondi M. *Top. Curre. Chem.* 1990; **153**: 41; (b) Gerratt J, Cooper DL, Karadakov B, Raimondi M. *Chem. Soc. Rev.* 1997; 87; (c) Gerratt J, Cooper DL, Raimondi M. In *Pauling's Legacy—Modern Modeling of the Chemical Bond*, Maksic ZB, Orville-Thomas WJ (eds). Elsevier: Amsterdam, 1999.
27. (a) Hiberty PC, Cooper DL. *J. Mol. Struct. (THEOCHEM)* 1988; **169**: 437; (b) McWeeny R. *Theor. Chim. Acta* 1988; **73**: 115.
28. (a) Rumer G. *Göttinger Nach*. 1932; 337; (b) Pauncz R. *The Symmetric Group in Quantum Chemistry.* CRC Press: New York, 1995; 124–125.
29. (a) Berry RS. *J. Chem. Phys.* 1959; **30**: 936; (b) Hiberty PC, Ohanessian G. *J. Am. Chem. Soc.* 1982; **104**: 66; (c) Hiberty PC, Ohanessian G. *Int. J. Quantum Chem.* 1985; **27**: 245, 249.
30. Hiberty PC. *J. Mol. Struct. (THEOCHEM)* 1998; **451**: 237.
31. (a) Zilberg S, Haas Y. *Int. J. Quantum Chem.* 1999; **71**: 133; (b) Zilberg S, Haas Y. *J. Phys. Chem. A* 1998; **102**: 10843.
32. (a) Shaik S, Shurki A, Danovich D, Hiberty PC. *J. Am. Chem. Soc.* 1996; **118**: 666; (b) Wu W, Danovich D, Shurki A, Shaik S. *J. Phys. Chem. A* 2000; **104**: 8744.

33. Mulder JJC, Oosterhoff LJ. *J. Chem. Soc., Chem. Commun*. 1970; 307.
34. (a) Kuwajima S. *J. Chem. Phys.* 1981; **74**: 6342; (b) Kuwajima S. *J. Chem. Phys.* 1982; **77**: 1930; (c) Kuwajima S. *J. Am. Chem. Soc.* 1984; **106**: 6496.
35. Maynau D, Malrieu J-P. *J. Am. Chem. Soc.* 1982; **104**: 3029.
36. (a) Shaik SS. In *New Concepts for Understanding Organic Reactions*, Betrán J, Csizmadia IG (eds). ASI NATO Series, vol. C267. Kluwer: Dordrecht, 1989; 165; (b) Wu W, Zhong S-J, Shaik S. *Chem. Phys. Lett.* 1998; **292**: 7–14.
37. Klein DJ, Zhu H, Valenti R, Garcia-Bach MA. *Int. J. Quantum Chem.* 1997; **65**: 421.
38. Heitler W, London F. *Z. Phys.* 1927; **44**: 455.
39. (a) Shaik S, Shurki A, Danovich D, Hiberty PC. *J. Am. Chem. Soc.* 1995; **117**: 7760; (b) Kutzelnigg W. In *Theoretical Models of Chemical Bonding*, vol. **2**, Maksic ZB (ed). Springer: Berlin, 1990; 1; (c) Wu W, Zhong S-J, Shaik S. *Chem. Phys. Lett.* 1998; **292**: 7.
40. (a) Dauben HJ, Jr, Wilson JD, Laity JL. *J. Am. Chem. Soc.* 1969; **91**: 1991; (b) Haberditzl W. *Angew. Chem.* 1966; **78**: 277; *Angew. Chem., Int. Ed. Engl.* 1966; **5**: 288.
41. Gogonea V, Schleyer P von R, Schreiner PR. *Angew. Chem.* 1998; **110**: 2045; *Angew. Chem., Int. Ed. Engl.* 1998; **37**: 1945.
42. (a) Atkins PW. *Molecular Quantum Mechanics* (2nd edn). Oxford University Press: Oxford, 1983; (b) Salem L. *The Molecular Orbital Theory of Conjugated Systems*. Benjamin: New York, 1966.
43. Wagniere G, Gouterman M. *Mol. Phys.* 1962; **5**: 621.
44. (a) Salem L, Roland C. *Angew. Chem. Int. Ed. Engl.* 1972; **11**: 92; (b) Shaik SS. *J. Am. Chem. Soc.* 1979; **101**: 3184; (c) Michl J. *J. Am. Chem. Soc.* 1996; **118**: 3568.
45. (a) Lefebvre-Brion H, Field RW. *Perturbations in the Spectra of Diatomic Molecules*. Academic Press: New York, 1986; (b) McGlynn SP, Azumi T, Kinoshita M. *Molecular Spectroscopy of the Triplet State*. Prentice-Hall: Englewood Cliffs, NJ, 1969; (c) Matsen FA, Klein DJ. *Adv. Photochem.* 1969; **7**: 1; (d) Richards WG, Trivedi HP, Cooper DL. *Spin–Orbit Coupling in Molecules*. Clarendon Press: Oxford, 1981.
46. Balková A, Bartlett RJ. *J. Chem. Phys.* 1994; **101**: 8972.
47. Lorentzon J, Malmqvist P-Å, Fülscher M, Roos BO. *Theor. Chim. Acta*, 1995; **91**: 91.